GRUMMAN AIRCRAFT ENGINEERING CORPORATION

ADVANCED DEVELOPMENT PROGRAM

STUDY ON PRESSURE DISTRIBUTIONS IN CONICAL NOZZLES

FINAL REPORT

Contract No. NAS 7-100, Task Order RD-32

JPL P.O. No. 369764

Report No. ADR 01-10-65.1 DATE: September 1965

LIBRARY COPY

AUG 3 1966

LANGLEY RESEARCH CENTER
LIBRARY, NASA
LANGLEY STATION
HAMPTON, VIRGINIA

BY D. Migdal

Propulsion Section

APPROVED BY _____
Chief of Propulsion

APPROVED BY _____
Director of Advanced Development

FOREWORD

This work was performed by the Grumman Aircraft Engineering Corporation for the Jet Propulsion Laboratory under contract NAS7-100. The scope of this work was prompted by JPL Technical Report No. 32-654 which contains experimentally determined wall pressure distribution in conical supersonic nozzles and discusses the validity of various analytical solutions and shock formation. In particular, the shock formation aspects stimulated the publication of a Technical Note in the A.I.A.A. Journal (Aug. 1965). For completeness, the results contained in the above note are incorporated into this report.

This document is unclassified.

TABLE OF CONTENTS

LIST OF TABLES

LIST OF ILLUSTRATIONS

INTRODUCTION

Previous analyses indicate that conventional conical nozzles are not shock free †[1,2] and that the initial shock formation occurs near the axis of symmetry[2]. There are several applications where the formation of a shock in this region is of importance. For example, conventional conical nozzles are often used to study nonequilibrium flow,[3,4] and there exists the possibility of obscuring the chemical effects with aerodynamic factors; in the study of flow over bodies placed along the centerline of wind tunnel nozzles the free stream conditions cannot be properly assessed without a knowledge of the effects of shock formation; and for the same reason the design of contoured wind tunnel nozzles based on the assumption of an initial source flow will not lead to completely predictable test section conditions.

Despite the practical significance, in the above applications, complete experimental verification of the shock formation is unavailable. It is the purpose of this report to discuss some of the physical phenomena which lead to the shock formation and to provide analytical predictions of the shock strength which can be used as the basis for experimental studies. Experimental studies will also be required to determine the extent to which the boundary layer modifies the calculated shock formation.

† List of references on page 6.

SUMMARY AND RECOMMENDATIONS

Many conical nozzles were analyzed. In all cases the crossing of Mach waves near the nozzle axis could be traced to the contour junction with the conical section. Continued calculations revealed a decay in the reflected shock strength, so that in most cases there was no discernible pressure rise along the contour. It thus appears that if the shock is to be detected experimentally it must be done by examining the interior of the flow, especially in the vicinity of the nozzle axis.

The static pressure along the axis for several conical nozzles appears in this report. This parameter appears to be the most easily measured experimental quantity. However the pressure rise occurs within a very limited region and therefore the shock location should be detected, initially, by visual observations (to determine pressure tap locations). The inclusion of a small circular pipe along the complete nozzle axis (for pressure instrumentation) will not materially affect the results contained in this report.

DISCUSSION

As used here, a conventional conical nozzle includes a cone attached directly to the throat (Fig. 1A) or a cone attached to a contour with constant radius of curvature (Fig. 1B). The assumptions and method of analysis outlined in Reference 5 were used here. The irrotational method of characteristics for axisymmetric flow was employed and numerical solutions were obtained with the IBM 7094. Crossing of the same family of Mach waves denoted the formation of a shock. The pressure rise is treated as an isentropic compression. This assumption yields a higher value of the shock strength (measured in terms of pressure ratio) than the use of oblique shock relations. For the flow deflections and Mach Numbers considered in this study the errors in pressure ratio were found to be less than 2%.

Exact shock relationships can be included without significantly complicating the numerical procedure in several cases. For example, in supersonic jet plumes the shock direction is towards the axis and characteristics procedures are available up to the point where the shock approaches the axis, or where normal shocks appear. Even in this case, however, the approximation used in this report yields satisfactory engineering results (as discussed below). Therefore the added complication required to include more exact shock relationships for continued weak shock reflections in nozzle flows does not appear warranted at this time.

The method outlined in reference 5 was extended to include an approximate kinetic analysis of the complete reacting gas flow through the nozzle and out into an exhaust plume. Since completely supersonic shocks always appear in the exhaust plume at low pressures, this type of flow field can be used to check the error introduced by not utilizing exact shock relationships. Because no other analysis of this type is presently available, the program results were compared with existing non-reacting analytical and unclassified experimental results. Typical comparisons for the near flow field, as shown in Figs. 2 and 3, are good and it can be safely assumed that the method will yield satisfactory results for flows in which chemical reaction play a significant role.

RESULTS

Typical results of the pressure distribution along the axis are shown in figure 4. The static pressure is divided by the chamber value, the distance (X) is referred to the throat radius (r_t), various circular arc radii of curvature (r_c) are joined to a 15° wall angle nozzle, and the ratio of specific heats (Gamma) was taken as 1.4. The results (Fig. 4) indicate that the pressure rise occurs within a very narrow region, and that increasing the throat radius of curvature shifts the axial location of the shock downstream and diminishes the shock strength.

The effect of increasing gamma and increasing the wall angle on the calculated origin of shock location have been studied. These results are consistent with the causes given below for the shock formation. That is, either effect taken independently increases the local Mach number slightly downstream of the throat; this decreases the magnitude of the slope of the right running waves (2-a in figure 1) and thereby displaces the shock formation region in the downstream direction.

Additional cases of interest are listed in Table 1 and the tabulated results appear in Tables 2-12. The wall and axis pressure distributions are shown graphically in figures 5-7 for cases C, D and E respectively. The general trend is a reduction in calculated shock strength and more nearly one-demensional flow as the nozzle wall angle is reduced.

In examining the region where the cone is attached to the contour (or directly to the throat) a discontinuous change in local radius of curvature is observed. This fact, by itself, gives no clue as to the cause of shock formation, since identical results with planar flow indicate shock free flow. The physical phenomena which lead to shock formation are thus due entirely to axisymmetric effects. In all cases, the calculation results reveal that downstream of the contour junction the streamlines near the wall are inclined at a larger flow angle than the wall itself (Fig. 1C). Thus, a compressive turning is required to satisfy the wall boundary conditions and this is the beginning of the shock formation.

With the nomenclature of figures 1A and 1B, lines 2a and 3a represent right and left running characteristics respectively and the expansion from point 1 to point 2 occurs at the beginning of the conical section. Then the flow angle at point "a" (θ_a) is found to be greater than the inviscid flow angle at the wall ($\theta_2 = \theta_w$). This overturning of the flow can be shown analytically with the following assumptions: assume region 1-2 shrunk to a point as in Fig. 1A, point 3 sufficiently close to point 1 so that flow conditions at both points are identical and that the initial flow is parallel ($\theta_1 = \theta_3 = 0$). Then a Prandtl-Meyer turn from θ_1 to θ_2 produces the right running expansion line 2a. Using a standard characteristic solution for point "a", the first order

difference scheme results in

$$\theta_a - \theta_2 = \left[\frac{\sin\theta_2 \sin\alpha_2 \tan\alpha_2}{\cos(\theta_2 - \alpha_2)}\right] \frac{\epsilon(x_a - x_2)}{y_2} \Bigg/ \left[\frac{W_1}{W_2}\tan\alpha_1 + \tan\alpha_2\right]$$

where W is velocity, α is the Mach angle, ϵ = 1 for axisymmetric flow and zero for planar flow. With the positive direction of θ in the anti-clockwise sense (Fig. 1a) the right-hand side of the above equation contains only positive terms. It follows then, that $\theta_2 = \theta_a$ in planar flow (as it should be) but that $\theta_a > \theta_2$ for axisymmetric flow.

In the design of shock free optimum shaped axisymmetric nozzles[6,7] an initial region of the supersonic contour is arbitrarily specified and the contour downstream of this region is determined. This downstream contour contains a slight increase in wall angle before turning the flow back toward the axial direction (to accommodate the overturning mentioned previously). This suggests that shock free conical nozzles can be obtained by attaching the cone tangent to the optimum shaped contour at any point downstream of the maximum wall angle. Our studies as well as the results contained in reference 2 indicate that this method eliminates the formation of shocks.

REFERENCES

1. Migdal, D., and Landis, F., "Characteristics of Conical Supersonic Nozzles," ARS J. 32, 1898-190 (1962).

2. Darwell, H. M., and Bradham, H., "Shock Formation in Conical Nozzles," AIAA J. 1, 1932-1934, (1963).

3. Lezberg, E. A., and Franciscus, L. C., "Effects of Exhaust Nozzle Recombination on Hypersonic Ramjet Performance: 1. Experimental Measurements," AIAA J. 1, 2071-2076, (1963).

4. Chen, C. J., "Experimental Investigation of Atomic Recombination in a Supersonic Nozzle," J. Fluid Mech., Vol. 17, 450-458, (Nov. 1963).

5. Migdal, D., "Chemical Nonequilibrium in Nozzle Flows," Grumman Aircraft Engineering Corporation, ADR-01-10-64.1, (1964).

6. Ahlberg, J. H., Hamilton, S. A., Migdal, D. and Nilson, E. N., "Truncated Perfect Nozzles in Optimum Nozzle Design," ARS J., 3, 614-620, (1961).

7. Rao, G. V. R., "Exhaust Nozzle Contour for Optimum Thrust," Jet Propulsion, 28, 377-382 (1958).

Case	θ	Gamma	r_c/r_t	r_e/r_t	A_e/A_t	X_e/r_t	Wall	Axis*
A_1	15°	1.35	2.0	1.95	3.8	3.81	x	
A_2	15°	1.4	2.0	1.95	3.8	3.81	x	
B_1	15°	1.35	.625	2.57	6.62	5.96	x	
B_2	15°	1.4	.625	2.57	6.62	5.96	x	x
C	10°	1.4	2.0	2.56	6.56	9.02	x	x
D	15°	1.667	2.0	4.48	20.	13.25	x	x
E	5°	1.667	4.0	3.34	11.1	26.9	x	x

*Calculated shock region along the axis is contained in the appendix

TABLE 1

CONICAL NOZZLES FOR WHICH TABULATED DATA APPEARS IN APPENDIX

Inputs: $\theta = 15^{\circ}$ $\quad r_c/r_t = 2.0$

$\gamma = 1.35$ $\quad r_e/r_t = 1.95$

Contour 1. Radius : $$\left(3. - \frac{r}{r_t}\right)^2 = 4. - (x/r_t)^2$$

2. Straight Section : $$\frac{r}{r_t} = .927 + .2679\ x/r_t$$

x/r_t	r/r_t	tan θ	Mach	P/P_o	A/A_t
0	1.0000	0.	1.01000	0.53070	1.0001
0.1188	1.0035	0.05952	1.20201	0.41918	1.0072
0.2523	1.0160	0.12715	1.36375	0.33729	1.0323
0.4091	1.0423	0.20896	1.55134	0.25777	1.0865
0.5921	1.0856	0.26790	1.70963	0.20324	1.1787
0.9960	1.1938	0.26790	1.84538	0.16479	1.4253
1.3692	1.2938	0.26790	1.97797	0.13375	1.6741
1.6486	1.3687	0.26790	2.07918	0.11385	1.8734
1.8896	1.4332	0.26790	2.16525	0.09919	2.0543
2.4044	1.5711	0.26790	2.34745	0.07396	2.4687
2.9084	1.7062	0.26790	2.51582	0.05637	2.9112
3.8099	1.9477	0.26790	2.79344	0.03611	3.7938

TABLE 2

CASE A_1 - CONTOUR CALCULATIONS

Inputs: $\theta = 15^{o}$ $\quad r_c/r_t = 2.0$
$\gamma = 1.40$ $\quad r_e/r_t = 1.95$

Contour Same as Case A_1

x/r_t	r/r_t	tan θ	Mach	P/P_o	A/A_t
0	1.0000	0	1.01000	0.52213	1.0001
0.1195	1.0036	0.05984	1.20644	0.40892	1.0072
0.2539	1.0162	0.12801	1.37357	0.32611	1.0327
0.4125	1.0430	0.21079	1.56974	0.24602	1.0879
0.5982	1.0873	0.26790	1.73198	0.19303	1.1822
1.0119	1.1981	0.26790	1.87565	0.15495	1.4355
1.3961	1.3010	0.26790	2.01712	0.12444	1.6928
1.6851	1.3784	0.26790	2.12600	0.10500	1.9002
1.9354	1.4455	0.26790	2.21920	0.09075	2.0896
2.4732	1.5896	0.26790	2.41819	0.06648	2.5269
3.0044	1.7319	0.26790	2.60444	0.04977	2.9996
3.8099	1.9477	0.26790	2.86823	0.03321	3.7937

TABLE 3

CASE A_2 - CONTOUR CALCULATIONS

Inputs: $\theta = 15^{o}$ $\quad r_c/r_t = 0.625$

$\gamma = 1.35$ $\quad r_e/r_t = 2.575$

Contour 1. Radius : $(1.625 - \frac{r}{r_t})^2 = .39 - (\frac{x}{r_t})^2$

2. Straight Section : $\frac{r}{r_t} = .977 + .2679 \frac{x}{r_t}$

x/r_t	r/r_t	tan θ	Mach	P/P_o	A/A_t
0.	1.0000	0.	1.01000	0.53070	1.0001
0.1502	1.0184	0.24798	1.58040	0.24692	1.0371
0.3147	1.0608	0.26790	1.66313	0.21812	1.1255
0.4917	1.1082	0.26790	1.71679	0.20103	1.2283
0.6844	1.1599	0.26790	1.77740	0.18314	1.3454
1.3806	1.3464	0.26790	2.02048	0.12502	1.8129
2.1038	1.5401	0.26790	2.28593	0.08168	2.3721
2.8131	1.7302	0.26790	2.53550	0.05461	2.9937
3.5548	1.9288	0.26790	2.77237	0.03735	3.7207
4.1643	2.0921	0.26790	2.95391	0.02800	4.3773
5.1882	2.3664	0.26790	3.2234	0.01838	5.6005
5.9570	2.5724	0.26790	3.40478	0.01392	6.6177

TABLE 4

CASE B_1 - CONTOUR CALCULATIONS

Inputs: $\theta = 15^{o}$ $\quad r_c/r_t = 0.625$
$\gamma = 1.40$ $\quad r_e/r_t = 2.575$

Contour Same as B_1

x/r_t	r/r_t	tan θ	Mach	P/P_o	A/A_t
0.	1.0000	0.	1.01000	0.52213	1.0001
0.1516	1.0187	0.25034	1.60095	0.23494	1.0378
0.3182	1.0618	0.26790	1.68302	0.20784	1.1274
0.4976	1.1098	0.26790	1.73907	0.19097	1.2318
0.6932	1.1622	0.26790	1.80253	0.17337	1.3508
1.4086	1.3539	0.26790	2.06125	0.11617	1.8331
2.1583	1.5547	0.26790	2.34813	0.07417	2.4173
2.9059	1.7550	0.26790	2.62389	0.04830	3.0803
3.6997	1.9677	0.26790	2.89090	0.03209	3.8720
4.364	2.1452	0.26790	3.09939	0.02347	4.6023
5.0768	2.3366	0.26790	3.30155	0.01744	5.4601
5.957	2.5724	0.26790	3.53374	0.01250	6.6178

TABLE 5

CASE B_2 - CONTOUR CALCULATIONS

x/r_t	P/P_o	Mach	
0.14043	0.52213	1.0100	
0.42248	0.43144	1.1651	
0.70081	0.32378	1.3787	
1.0202	0.22036	1.6440	
1.3434	0.14458	1.9205	
1.5194	0.11379	2.0745	
2.3064	0.045534	2.6621	
3.1621	0.019623	3.2207	
3.6581	0.013532	3.4778	*
3.7374	0.042054	2.7137	*
3.7781	0.052398	2.5712	*
3.8099	0.045577	2.6615	
4.4959	0.031927	2.8943	
5.2123	0.024838	3.0613	
5.9275	0.019189	3.2359	

* Region of Shock Location

TABLE 6

CASE B_2 - NOZZLE AXIS CALCULATIONS

Inputs: $\theta = 10^{o}$ $\quad r_c/r_t = 2.0$
$\gamma = 1.40$ $\quad r_e/r_t = 2.56$

Contour 1. Radius : $(3. - \frac{r}{r_t})^2 = 4. - (\frac{x}{r_t})^2$

2. Straight Section : $\frac{r}{r_t} = .971 + .1763 \frac{x}{r_t}$

x/r_t	r/r_t	tan θ	Mach	P/P_o	A/A_t
0.	1.0000	0.	1.01000	0.52213	1.0001
0.2539	1.0162	0.12801	1.37357	0.32611	1.0327
0.5878	1.0746	0.17630	1.55082	0.25296	1.1549
1.3072	1.2015	0.17630	1.77384	0.18113	1.4436
1.7797	1.2848	0.17630	1.93307	0.14180	1.6507
3.5766	1.6016	0.17630	2.49213	0.05925	2.5652
5.7458	1.9840	0.17630	2.98255	0.02795	3.9365
6.4642	2.1106	0.17630	3.04934	0.02593	4.4551
6.4702	2.1117	0.17630	3.03256	0.02593	4.4596
6.5077	2.1183	0.17630	3.03542	0.02582	4.4876
7.7326	2.3343	0.17630	3.22351	0.01954	5.4492
9.0200	2.5612	0.17630	3.42739	0.01454	6.5604

TABLE 7

CASE C - CONTOUR CALCULATIONS

x/r_t	P/P_o	Mach
.14036	0.52213	1.0100
.97131	0.26373	1.5223
1.5591	0.14232	1.9307
2.4124	0.062628	2.4565
2.4820	0.060749	2.4761
2.5511	0.085804	2.2550*
2.7680	0.093715	2.1987
2.8138	0.093353	2.2012
3.8916	0.066679	2.4163
5.8362	0.033130	2.8699
7.7876	0.018160	3.2736
8.9617	0.013416	3.4838

* Region of Shock Location

TABLE 8

CASE C - NOZZLE AXIS CALCULATIONS

Inputs: $\theta = 15^{o}$ $\quad r_c/r_t = 2.0$
$\gamma = 5/3$ $\quad r_e/r_t = 4.48$

Contour 1. Radius : $(3. - \frac{r}{r_t})^2 = 4. - (x/r_t)^2$

2. Straight Section : $\frac{r}{r_t} = .927 + .2679\frac{x}{r_t}$

x/r_t	r/r_t	tan θ	Mach	P/P_o	A/A_t
0	1.0000	0.	1.0100	0.48103	1.0001
0.1442	1.0052	0.07229	1.26144	0.34509	1.0105
0.4309	1.0470	0.22064	1.67773	0.19117	1.0962
1.1013	1.2220	0.26790	2.05473	0.11121	1.4935
1.8970	1.4352	0.26790	2.41654	0.06710	2.0600
3.6177	1.8962	0.26790	3.21584	0.02398	3.5958
6.1326	2.5699	0.26790	4.27814	0.00745	6.6
8.0469	3.0828	0.26790	5.00281	0.00375	9.5042
10.033	3.6149	0.26790	5.6947	0.00208	13.0686
12.1067	4.1704	0.26790	6.37179	0.00124	17.3933
13.2500	4.4767	0.26790	6.72442	0.00097	20.0420

TABLE 9

CASE D - CONTOUR CALCULATIONS

x/r_t	P/P_o	Mach	
0.14036	0.48103	1.0100	
1.0394	0.21082	1.6098	
1.6494	0.10532	2.0931	
2.0823	0.064102	2.45	
2.6887	0.034195	2.9284	
3.5148	0.016036	3.5598	
4.7383	0.0062695	4.4519	
5.0289	0.0050908	4.6693	*
5.5468	0.010123	3.9798	
5.17377	0.014867	3.6268	
5.8160	0.013511	3.7127	
5.8966	0.012241	3.8027	
5.9797	0.011046	3.8978	
8.1610	0.0055151	4.5848	
11.278	0.0023952	5.52590	
13.178	0.0015311	6.0918	

* Region of Shock Location

TABLE 10

Case D - Nozzle Axis Calculations

Inputs: $\theta = 5^{o}$ $\quad r_c/r_t = 4.0$
$\gamma = 5/3$ $\quad r_e/r_t = 3.33$

Contour 1. Radius : $(5. - \frac{r}{r_t})^2 \quad 16 - (\frac{x}{r_t})^2$

2. Straight Section : $\frac{r}{r_t} \quad .9835 + .0875 \frac{x}{r_t}$

x/r_t	r/r_t	tan θ	Mach	P/P_o	A/A_t
0	1.0000	0.0	1.01000	0.48103	1.0001
0.2506	1.0079	0.06277	1.24682	0.35208	1.0159
0.8402	1.0570	0.08750	1.44121	0.26836	1.1174
1.5038	1.1151	0.08750	1.63601	0.20302	1.2435
3.9490	1.3290	0.08750	2.19777	0.09085	1.7665
5.4946	1.4643	0.08750	2.49485	0.06032	3.1443
8.9555	1.7671	0.08750	3.09140	0.02790	3.1229
11.5910	1.9977	0.08750	3.36646	0.02005	3.9911
11.6182	2.0001	0.08750	3.37180	0.01992	4.0007
11.7531	2.0119	0.08750	3.40849	0.01908	4.0480
11.8998	2.0247	0.08750	3.44244	0.01835	4.0999
11.7116	2.0083	0.08750	3.8022	0.01973	4.0334
11.9078	2.0254	0.08750	3.42569	0.01872	4.1027
15.9780	2.3816	0.08750	4.02123	0.00969	5.6723
20.4688	2.7745	0.08750	4.57842	0.00555	7.6985
23.2079	3.0142	0.08750	4.84469	0.00417	9.0860
26.8999	3.3372	0.08750	5.27034	0.00297	11.1380

TABLE 11

CASE E - CONTOUR CALCULATIONS

x/r_t	P/P_o	Mach	
.14036	.48103	1.01	
.65195	.34027	1.2717	
1.0144	.24965	1.4920	
1.6946	.14739	1.8580	*
1.7507	.16510	1.7793	
1.9166	.17403	1.7428	
2.3191	.16005	1.8009	
2.8872	.13158	1.937	
3.8017	.093708	2.1758	
4.5819	.07157	2.3695	
5.8273	.050075	2.6339	
6.6222	.043584	2.7395	*
6.8749	.061616	2.4792	
6.9492	.06283	2.4648	
7.575	.042896	2.7517	
8.8929	.030600	3.0169	
10.407	.02245	3.2708	
12.242	.015940	3.5651	
14.127	.011927	3.8266	
16.040	.0093577	4.0549	
19.846	.006977	4.3431	*
19.981	.011779	3.8381	
20.507	.007468	4.2751	
22.072	.0051314	4.6608	
24.086	.003939	4.948	
26.900	.0029391	5.2820	

* Region of Shock Locations

TABLE 12

CASE E - NOZZLE AXIS CALCULATIONS

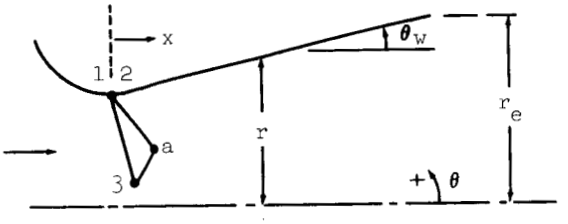

1A. Sharp Corner

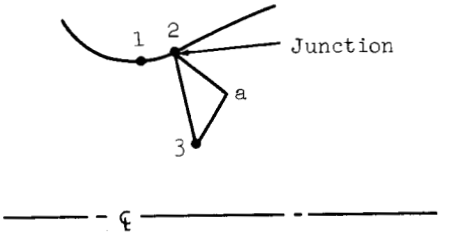

1B. Radius Of Curvature

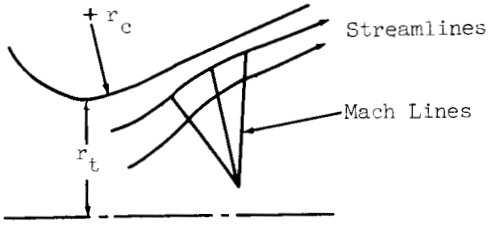

1C. Schematic

Fig. 1 Flow Field And Nomenclature

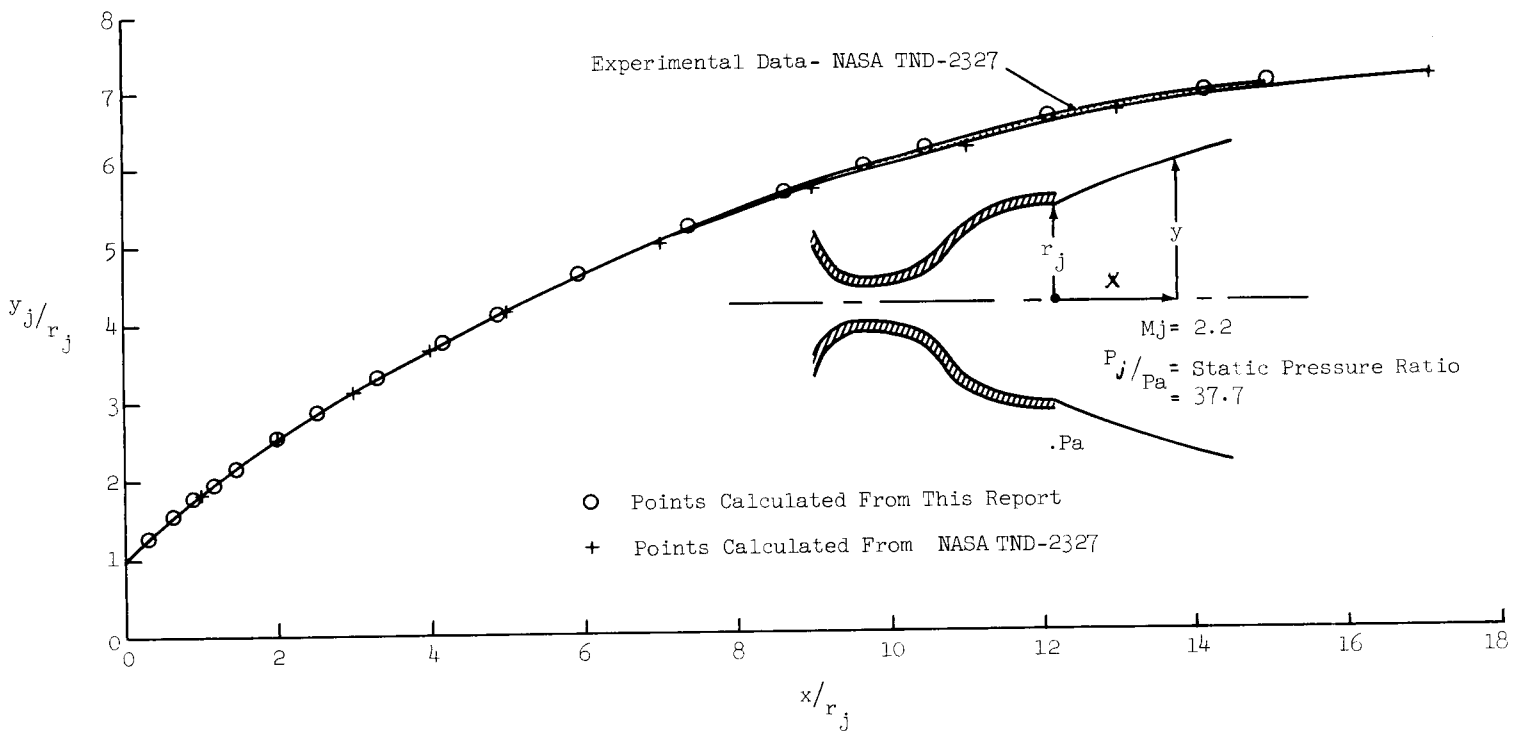

Fig. 2 Comparison Of Jet Plume Boundaries - C-D Nozzle

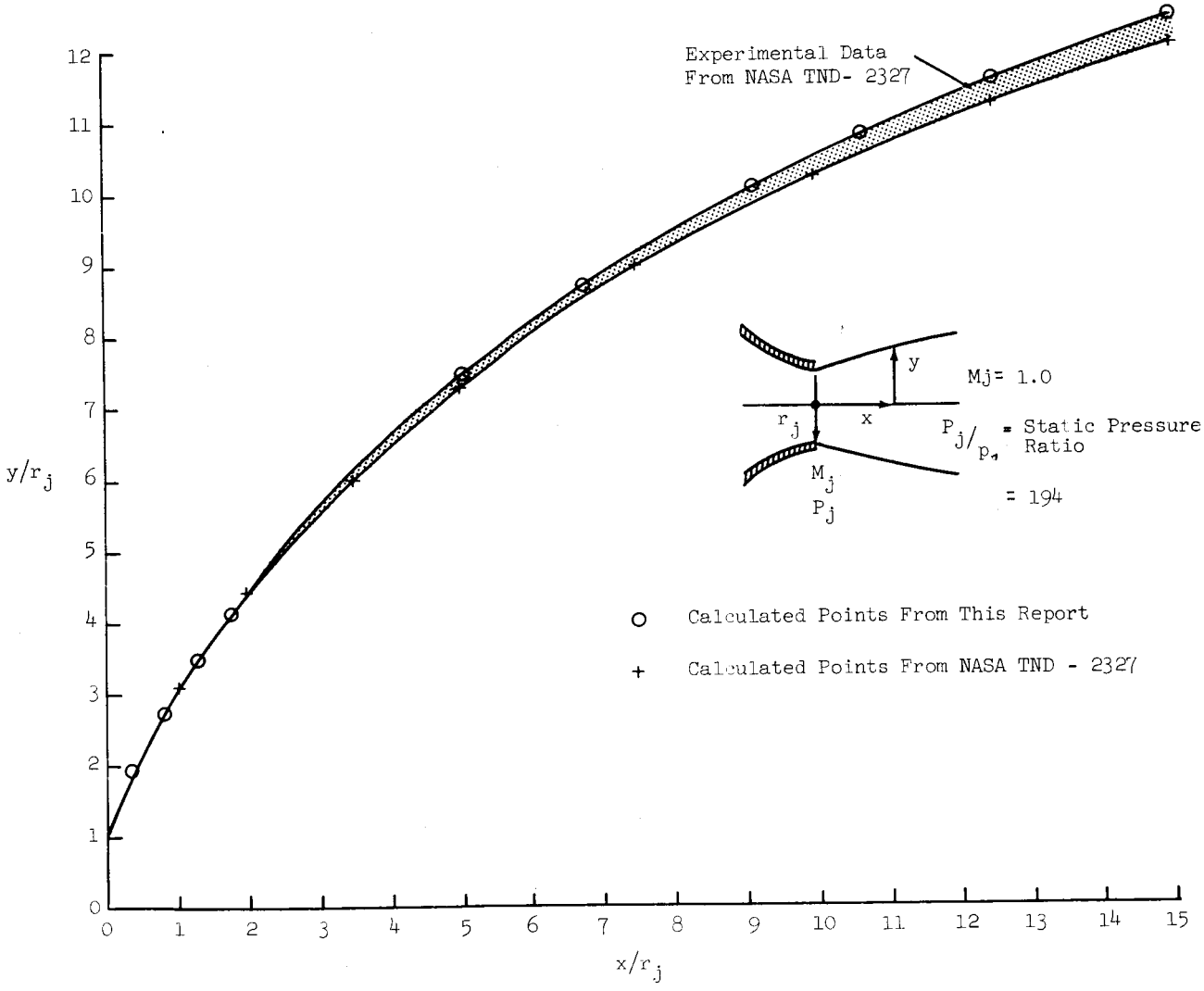

Fig. 3 Comparison Of Jet Plume Boundaries - Conv. Nozzle

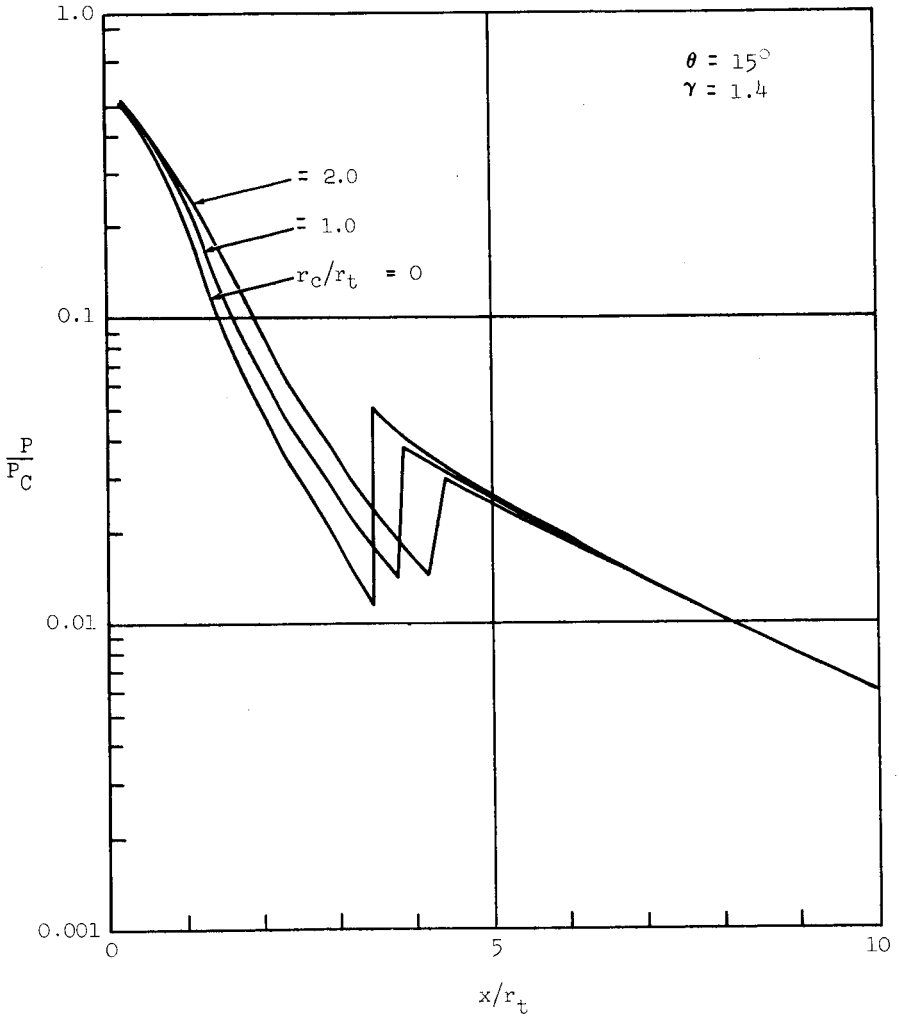

Fig. 4 Effect Of Radius Of Curvature Shock Strength And Location

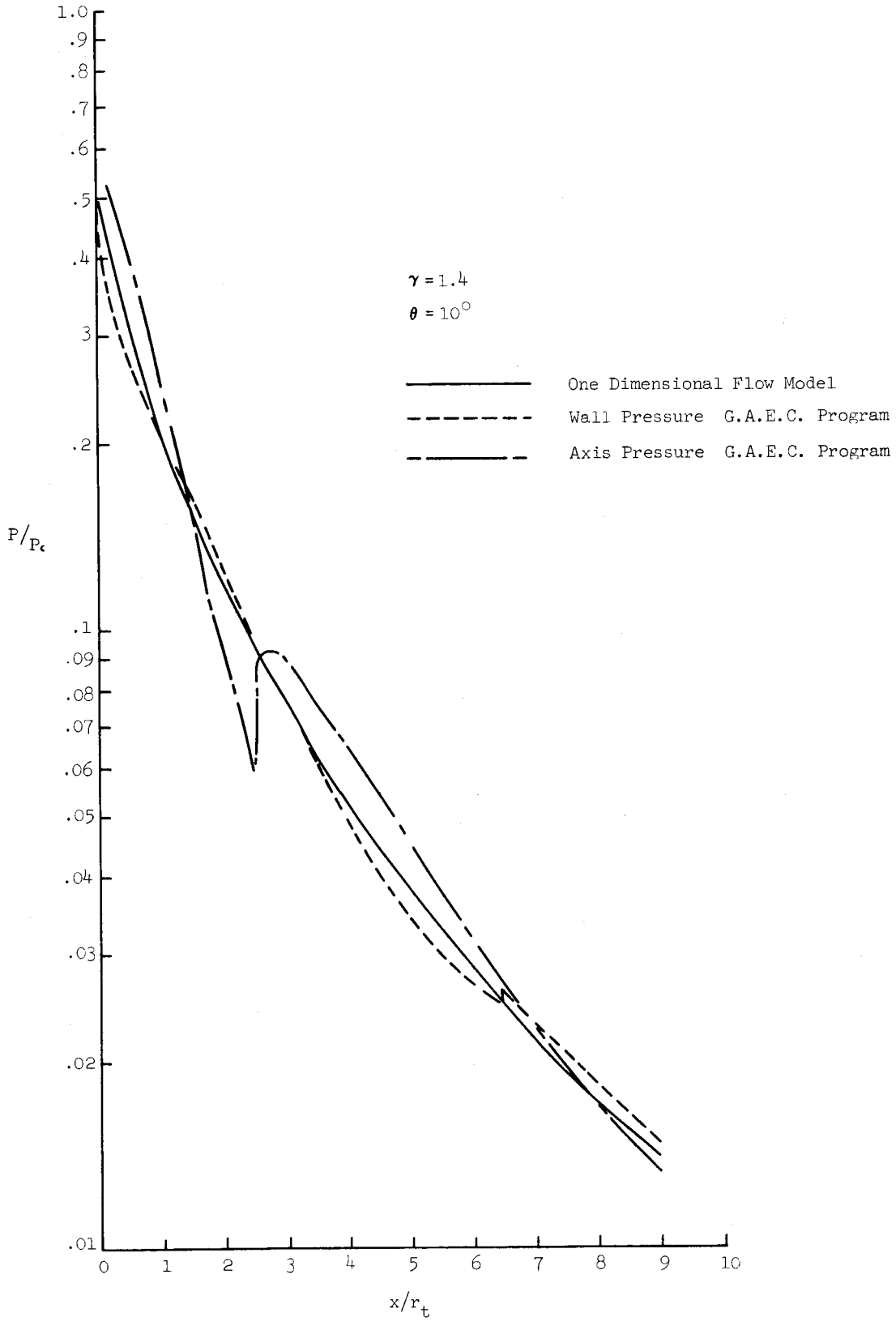

Fig. 5 Conical Nozzle Pressure Distributions
Case "C"

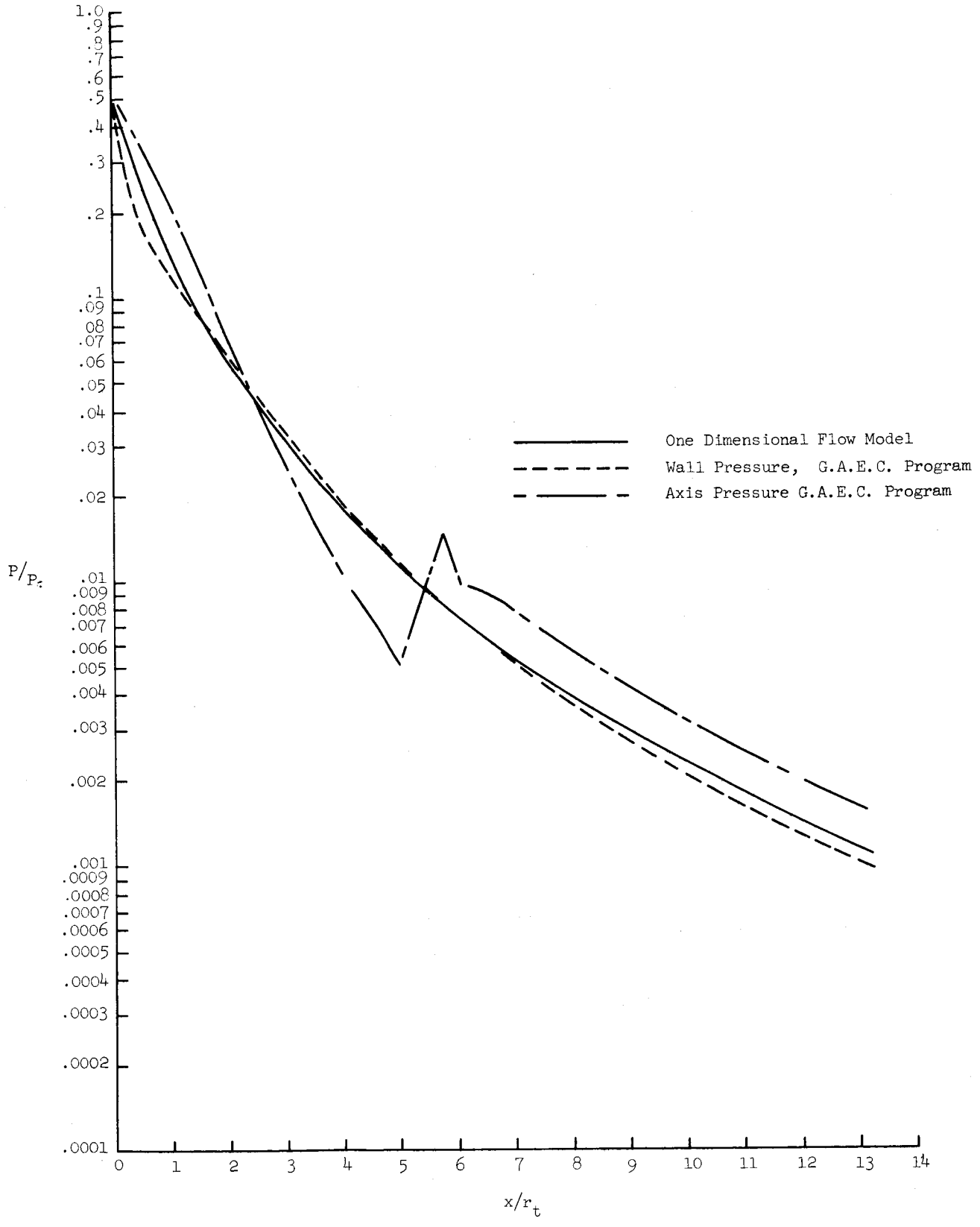

Fig. 6 Conical Nozzle Pressure Distributions
Case D: θ = 15°, γ = 1.667

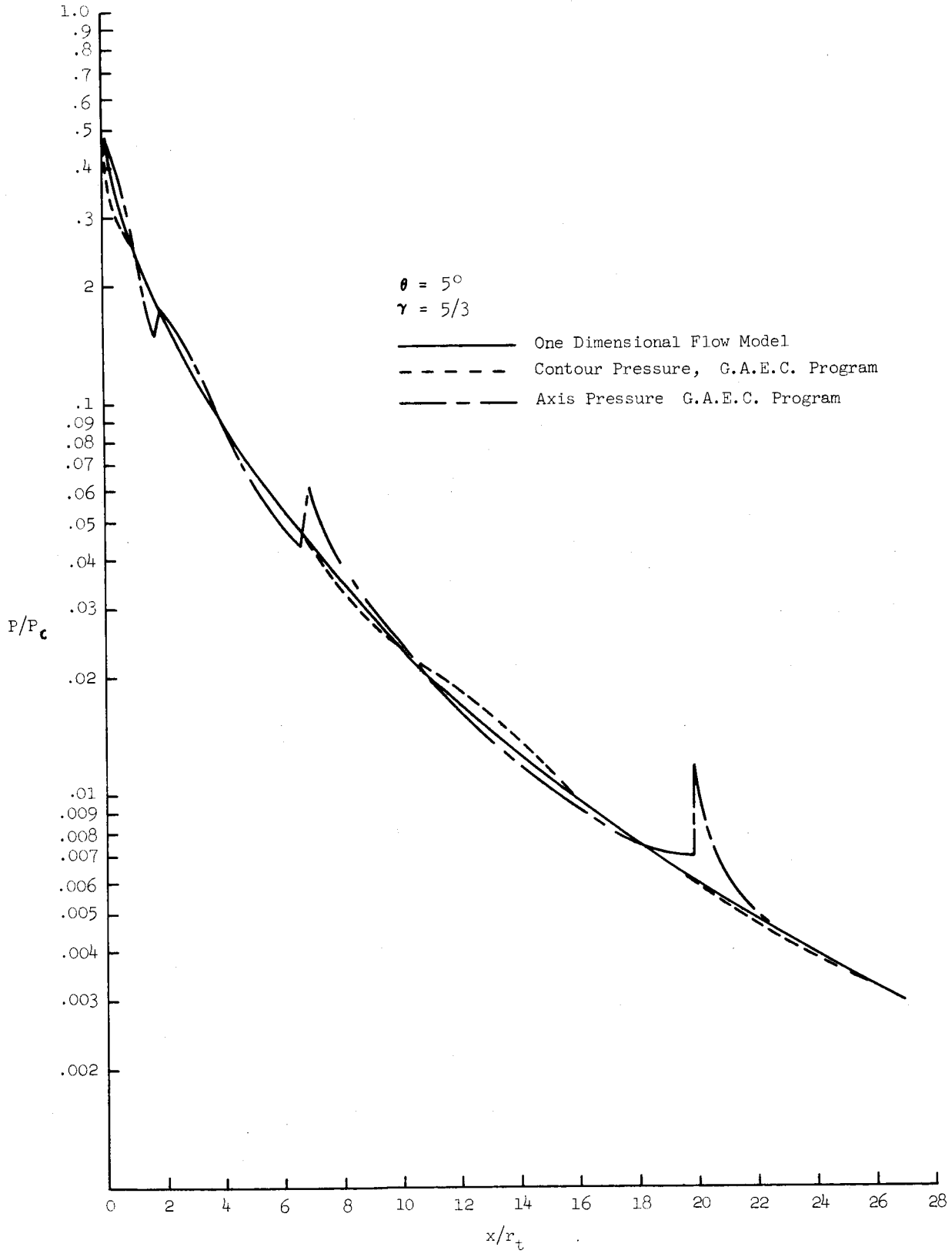

Fig. 7 Conical Nozzle Pressure Distributions Case E